Supplementary figures

S. Figure 1

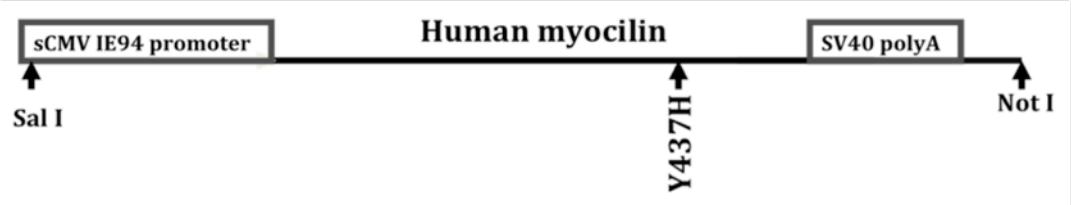

S. Figure 1: Schematic of T*g-MYOC*^{Y437H} construct. We generated transgenic mice carrying a mutation of human *MYOC* (*Y437H*) under the control of the CMV promoter.

S. Figure 2

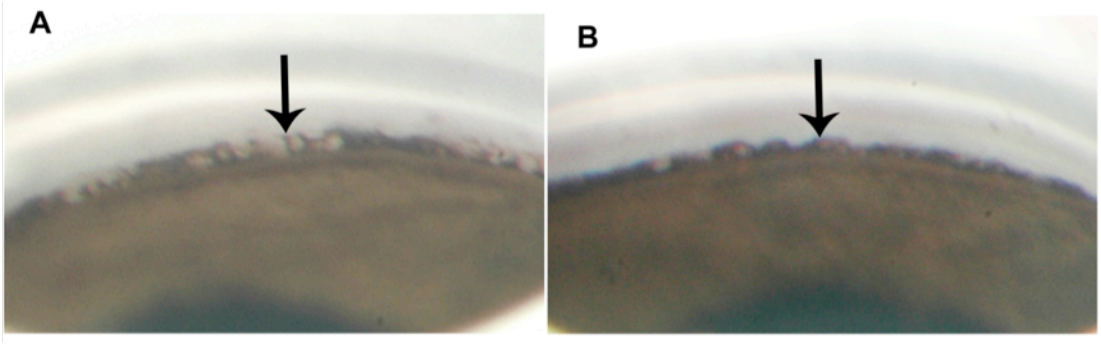

S. Figure 2: Open iridocorneal angle and normal morphology of anterior chamber structures in T*g-MYOC*^{Y437H} mice. Normal fine iris strands were apparent and the angle was free of debris or other abnormalities in **(B)** T*g-MYOC*^{Y437H} mice compared to **(A)** WT littermates as assessed by gonioscopy. Arrows show attachment of iris to trabecular meshwork.

S. Figure 3

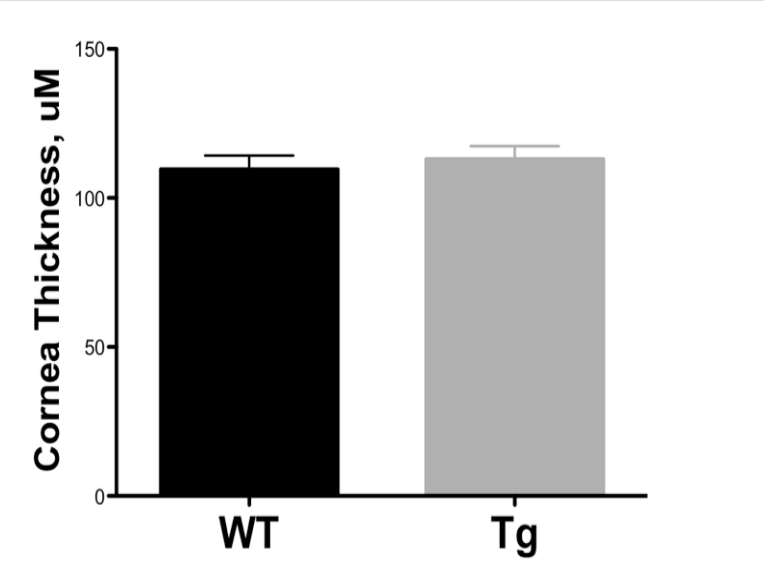

S. Figure 3: Normal corneal thickness in T*g-MYOC*^{Y437H} mice. Corneal thickness (uM) of T*g-MYOC*^{Y437H} mice (*n*=4) was compared to WT littermates (*n*=3).

S. Figure 4 **A**

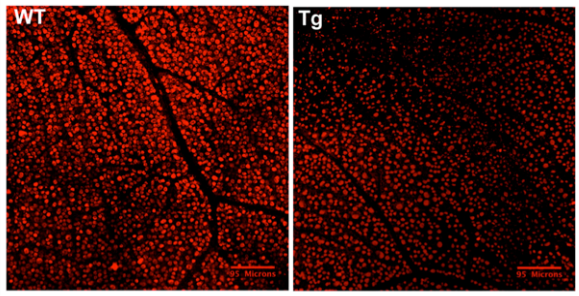

B

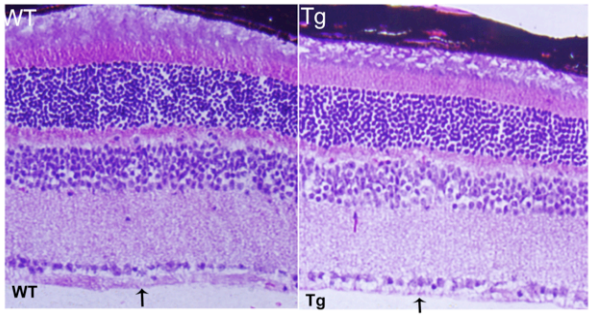

S. Figure 4: Loss of RGCs in the T*g-MYOC*^{Y437H} mice. A) Whole mount retinal preparations were stained with gamma synuclein antibody. Representative confocal images from 5-month-old WT and T*g-MYOC*^{Y437H} littermates are showing loss of RGCs in T*g-MYOC*^{Y437H} mice. Five-month-old T*g-MYOC*^{Y437H} mice have fewer RGCs compared to WT littermates. The loss of RGCs in T*g-MYOC*^{Y437H} mice preferentially occurred in the periphery of the retina. **B)** H & E stained sagital sections of retina of 5-months-old WT and T*g-MYOC*^{Y437H} littermates showing that retinal layers of T*g-MYOC*^{Y437H} mice are structurally similar to WT littermates.

S. Figure 5

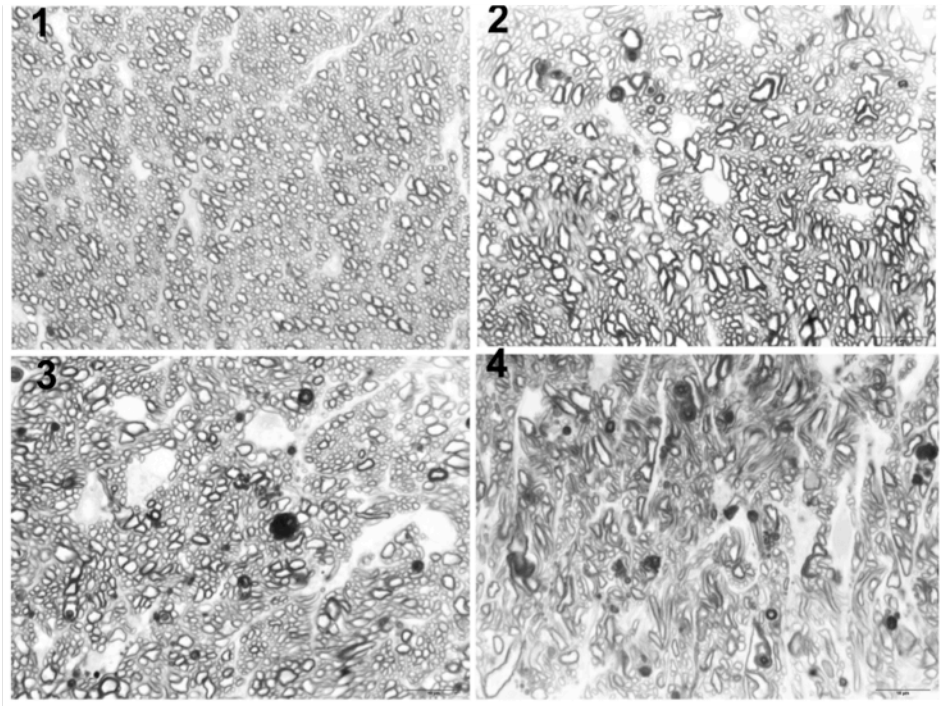

S. Figure 5: Optic nerve degeneration of T*g-MYOC*^{Y437H} mice. Representative images of PPD stained optic nerve sections showing normal (1), mild (2), moderate (3), and severe (4) axonal degeneration in T*g-MYOC*^{Y437H} mice.

S. Figure 6

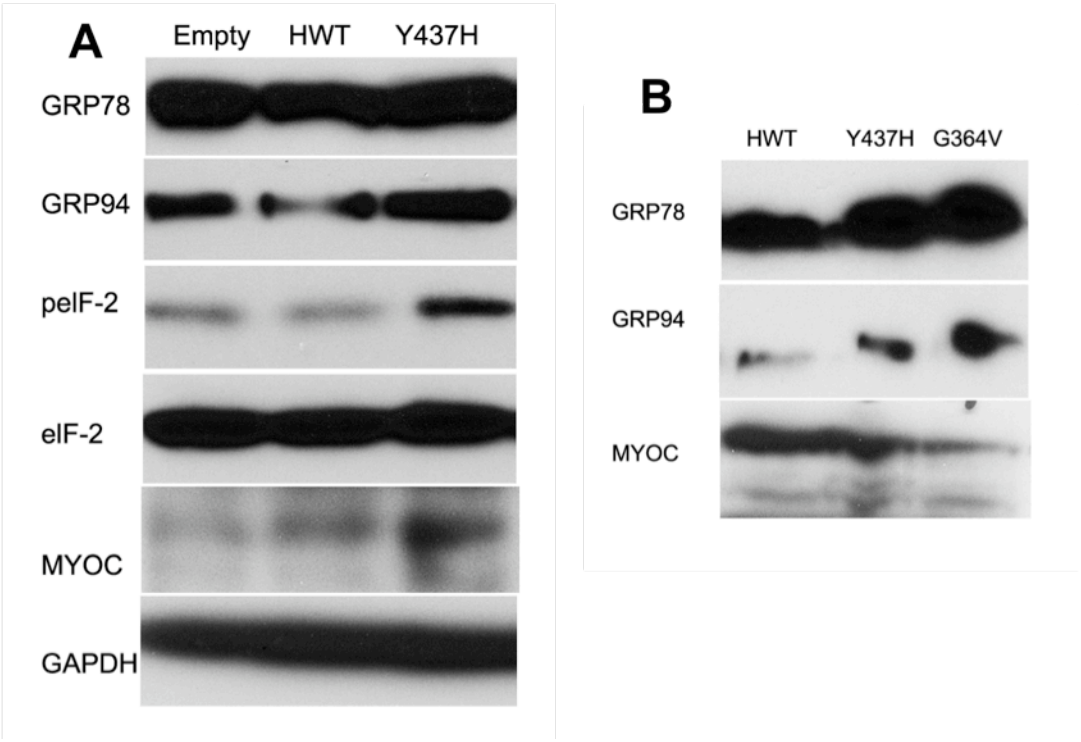

S. Figure 6: Expression of Y437H MYOC induces ER stress in cultured TM cells. A) Primary human TM cells were infected with empty adenovirus or viruses expressing WT or Y437H MYOC. After 6 days of culture, TM cell lysates were subjected to western blot analysis of ER stress markers. Expression of only Y437H MYOC and not WT MYOC induced ER stress in cultured TM cells. **A)** TM-5 cells were infected with empty adenovirus or viruses expressing WT or Y437H MYOC or G346V MYOC. Cell lysates were examined for GRP78, GRP94 and myocilin by western blot analysis. Expression of mutant myocilin (both Y437H MYOC and G346V MYOC) increased GRP78 and GRP94, indicating induction of ER stress.

S. Figure 7

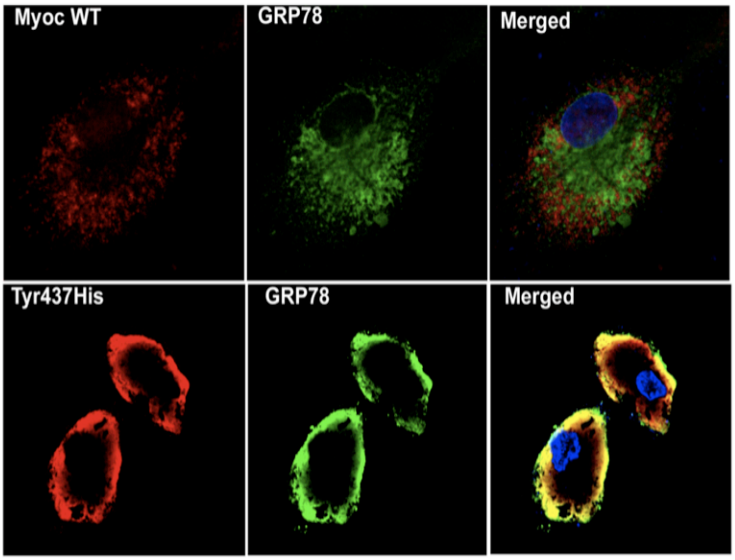

S. Figure 7: Mutant MYOC accumulates in the ER of primary TM cells. WT or mutant myocilin was expressed in primary TM cells and colocalization of myocilin with ER marker GRP78 was studied using confocal microscopy. WT myocilin appears to be transiently associated with GRP78. However, mutant myocilin was completely colocalized with GRP78 indicating its accumulation in the ER.

S. Figure 8

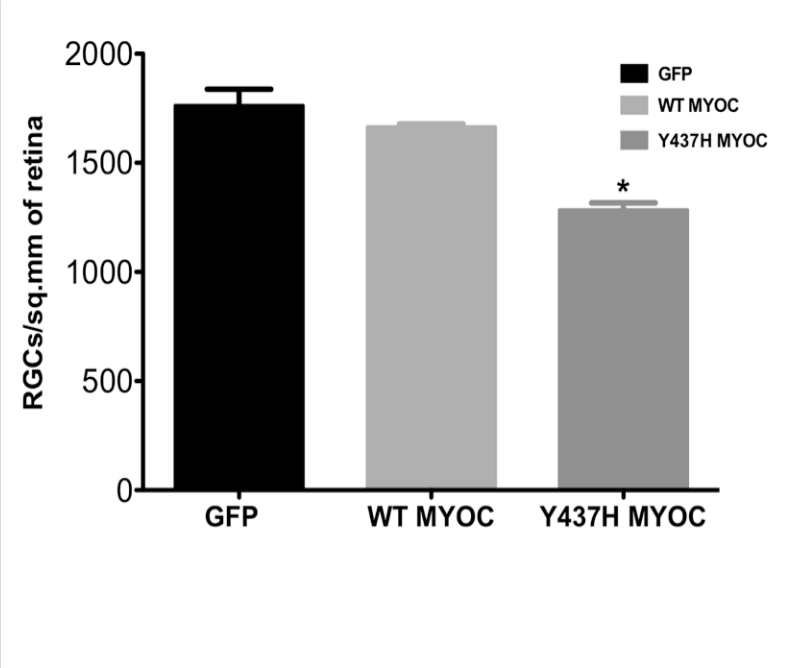

S. Figure 8: Y437H MYOC expression in the TM leads to loss of RGCs in C57BL/6J mice. C57BL/6J mice injected with adenovirus expressing GFP, WT or Y437H MYOC, which selectively transduce TM tissues. Mice were sacrificed 2 months post injections. RGCs were counted from whole mount retinas stained with gamma synuclein antibody.

S. Figure 9

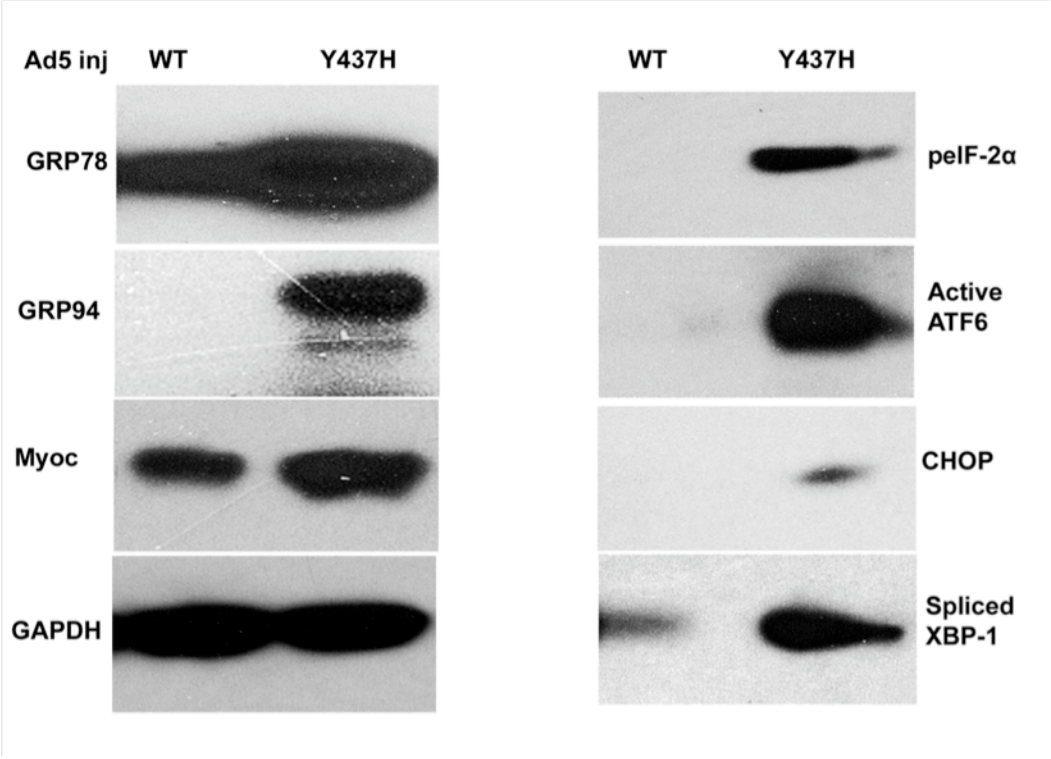

S. Figure 9: Increased ER stress markers in the anterior segment tissues of T*g-MYOC*^{Y437H} mice. Increased ER stress markers including GRP78, GRP94, spliced XBP-1, activated ATF-6α, and peIF-2α, were detected in 12-months-old T*g-MYOC*^{Y437H} anterior segment tissues by western blot.

S. Figure 10

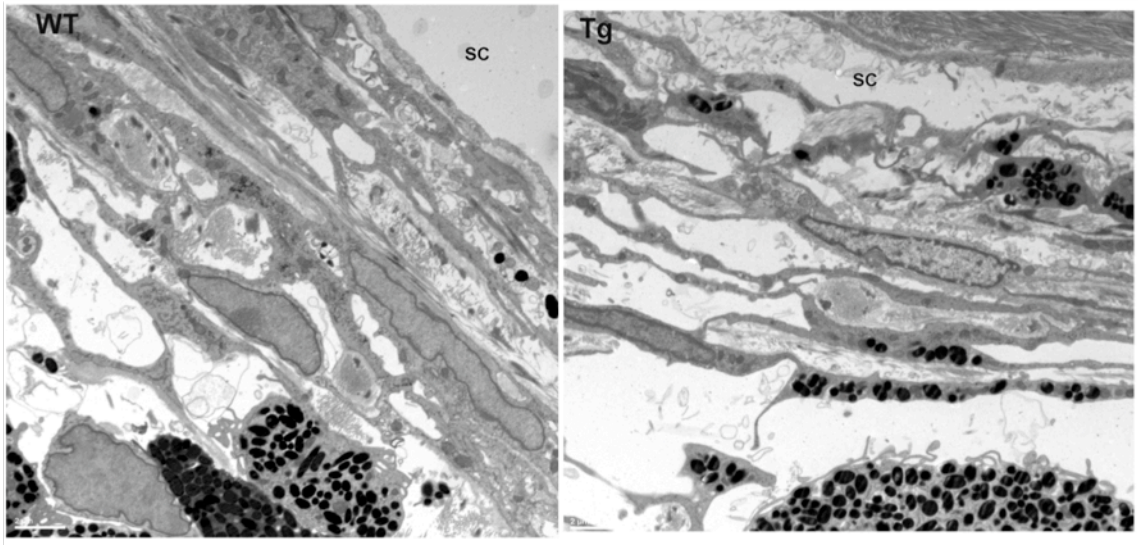

S. Figure 11: Representative TEM image of trabecular meshwork cells in WT (left) and T*g-MYOC*^{Y437H} mice (right). Loss of TM cells in 12-month-old T*g-MYOC*^{Y437H} mice examined by TEM analysis in WT (*n*=5) and T*g-MYOC*^{Y437H} mice (*n*=6). Less numbers of TM cells were observed in the T*g-MYOC*^{Y437H} mice.

S. Figure 11

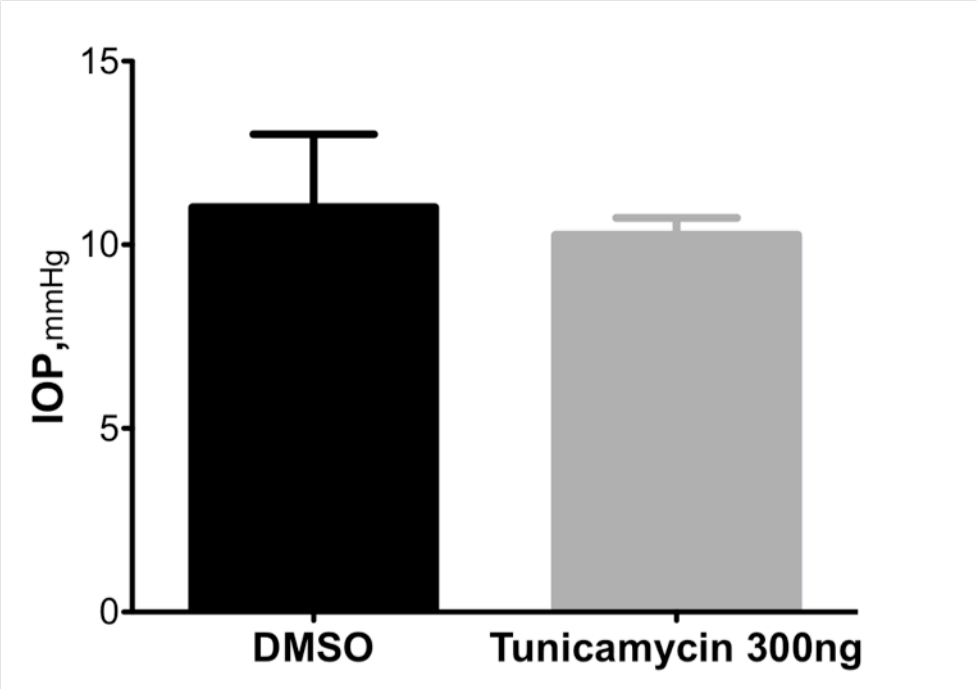

S. Figure 11: IOP measurements after 24 hours intracameral injection of tunicamycin. 4-months-old C57BL6 mice were injected with 300ng tunicamycin (3ul) or 3ul DMSO vehicle control. IOP were measured 24 hours after injections. Tunicamycin did not elevate IOP 24 hours after injections compared to vehicle control.

S. Figure 12

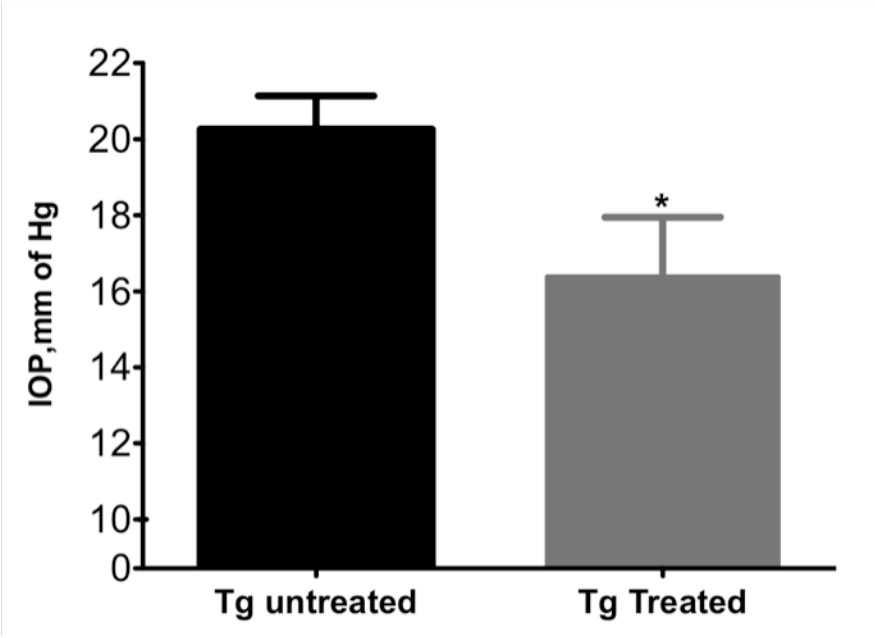

S. Figure 12: PBA treatment reduces IOP in 12-month-old *Tg-MYOC^{Y437H}* mice. 12-month-old T*g-MYOC^{Y437H}* mice were treated with PBA (20mM, ~10mg/mouse/day) in drinking water for 5 weeks and glaucoma phenotypes were compared to untreated littermates. n= 6 untreated and 8 treated T*g-MYOC^{Y437H}*, *$p< 0.04$ vs untreated. Data are mean ± s.e.m.

S. Figure 13

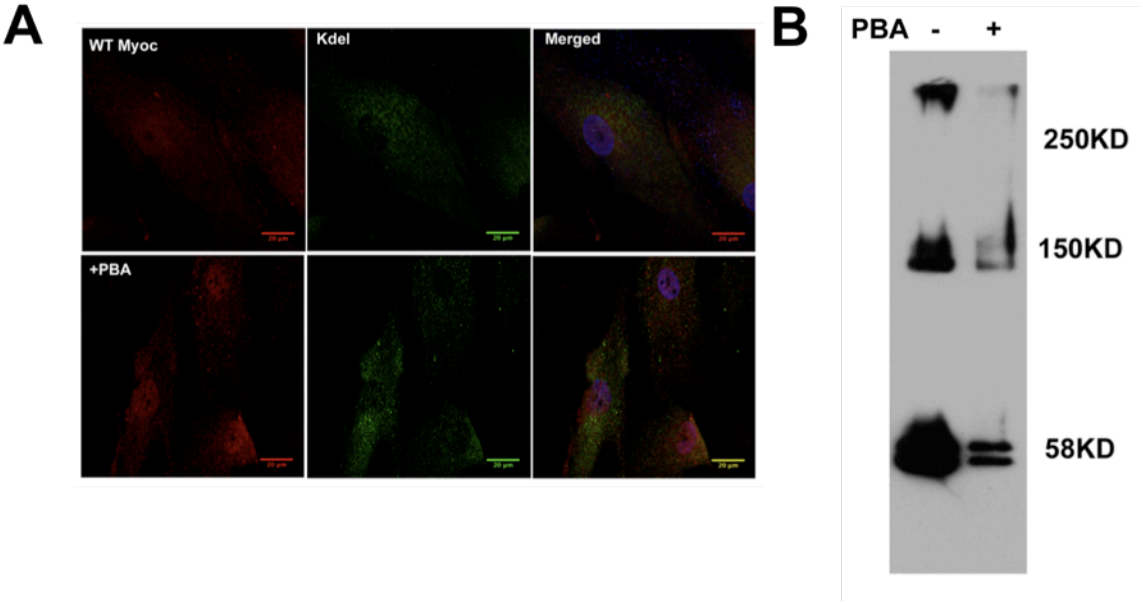

S. Figure 13: Effect of PBA treatment on MYOC localization and soluble aggregate formation. A) WT MYOC was expressed in primary TM cells using adenovirus and treated with PBA (5mM) for 5 days. Colocalization of WT MYOC (red) with ER marker KDEL (green) was studied by immunostaining. **B)** Western blot analysis of MYOC aggregates was examined after PBA treatment. TM cells expressing Y437HMYOC were lysed in buffer containing 0.5% triton and soluble proteins were run under reducing conditions. MYOC antibody detected higher molecular weight bands at 145 KD and above 250KD indicating MYOC soluble aggregates as previously shown in other studies. PBA treatment reduced MYOC aggregates in TM cells expressing Y437H mutant of MYOC.

S. Figure 14

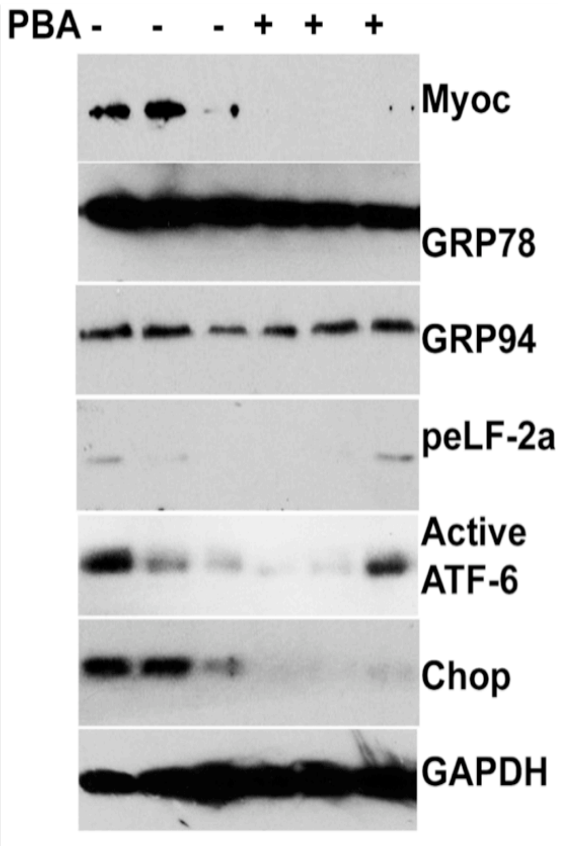

S. Figure 14: PBA treatment reduces ER stress in the iridocorneal angle of *Tg-MYOC^{Y437H}* mice: Western blot analysis of ER stress markers in the iridocorneal angle of *Tg-MYOC^{Y437H}* mice treated with PBA were compared with untreated *Tg-MYOC^{Y437H}* mice. PBA treatment reduced GRP78, GRP94, phosphorylated eIF2α, activated ATF-6α, and CHOP in *Tg-MYOC^{Y437H}* mice. PBA also reduced intracellular myocilin levels compared to untreated *Tg-MYOC^{Y437H}* mice.